

Entangled Orbital Triplet Pairs in Iron-Based Superconductors

T. Tzen Ong ¹, P. Coleman ^{1,2} and J. Schmalian ^{3,4}

¹*Center for Materials Theory, Department of Physics and Astronomy, Rutgers University, 136 Frelinghuysen Rd., Piscataway, NJ 08854-8019, USA*

²*Department of Physics, Royal Holloway University of London, Egham, Surrey TW20 0EX, UK.*

³*Institute for Theory of Condensed Matter, KIT, 76131 Karlsruhe, Germany.*

⁴*DFG Center for Functional Nanostructures, KIT, 76128 Karlsruhe, Germany.*

A key question in high temperature iron-based superconductivity is the mechanism by which the paired electrons minimize their strong mutual Coulomb repulsion. While electronically paired superconductors generally avoid the Coulomb interaction through the formation of nodal, higher angular momentum pairs, iron based superconductors appear to form singlet s-wave (s^\pm) pairs. By taking the orbital degrees of freedom of the iron atoms into account, here we argue that the s^\pm state in these materials possesses internal d-wave structure, in which a relative d-wave ($L = 2$) motion of the pairs entangles with the ($I = 2$) internal angular momenta of the d-orbitals to form a low spin $J = L + I = 0$ singlet. We discuss how the recent observation of a nodal gap with octahedral structure in KFe_2As_2 ^{1,2} can be understood as a high spin ($J = L + I = 4$) configuration of the orbital and isospin angular momenta; the observed pressure-induced phase transition into a fully gapped state² can then interpreted as a high-to-low spin phase transition of the Cooper pairs.

The family of iron-based high temperature superconductors exhibits a marked absence of nodes in the pair wavefunction^{3–15}. This stands in stark contrast with almost all other strongly correlated superconductors and superfluids, including the cuprates, heavy fermions, ruthenates and ^3He ^{16–30}, where the repulsive interaction between fermions drives the formation of higher angular momentum pairs with nodes in the pair wavefunction. In distinction, the Fe-based superconductors are generally believed to have an isotropic s^\pm structure. The underlying concern, voiced by Lev D. Landau[see: V. L. Ginzburg, About Science, Myself and Others CRC Press (2004)], that one cannot repeal Coulomb’s law must therefore find a new resolution in the Fe-based systems and other unconventional superconductors with multiple orbitals. In this context it is interesting that recent experiments^{1,2,31–36} show that upon doping, the gap structure can undergo a sudden transformation into an anisotropic paired state, suggesting the formation of higher angular momentum pairs. Is this a consequence of a competition between s-wave and higher angular momentum channels, or can a single unifying pairing mechanism account for these disparate experimental results? Here we show the existence of such a mechanism. By taking into account the unique helical orbital structure of the electronic bands, we show that an underlying d -wave orbital triplet can give rise to a new type of s^\pm state. Furthermore, we show that transformations in the relative orientation of the orbital and atomic isospin angular momenta of the pairs can account for the observed transition from an isotropic s^\pm -wave to an octet gap structure. An implication of our mechanism is that the origin of the pairing state is in the formation of hidden d -wave pairing.

The key to our theory lies in the helical orbital structure of the electronic bands, in which the orbital character of the quasiparticles behaves as a vector in orbital space, rotating twice as

one passes around the Γ point in the Brillouin zone³⁷, as shown in Fig. 1. This topologically non-trivial band structure is well established from first-principles calculations³⁸ and has been independently confirmed by ARPES measurements in both the normal state^{39,40} and the spin-density wave phase^{41,42}. The dominant atomic orbital character of Bloch waves near the Fermi surface involves the three t_{2g} orbitals, i.e. the xz , yz and xy orbitals⁴³. To illustrate the key elements of our theory, we adopt a simplified two orbital (xz/yz) model which captures the orbital helicity of the bands^{37,44}; later inclusion of the xy orbitals does not change the key conclusions. The xz and yz orbitals form a degenerate doublet or “iso-spin” which we label with the I_z index, treating the xz orbital as an “up” state with $I_z = +1$ and the yz orbital as a “down” state with $I_z = -1$. The electrons in these orbitals carry internal $L = 2$ angular momentum, containing a mixture of $M_z = \pm 1$ states. There are thus two potential sources of angular momentum carried by the Cooper pairs: external (\hat{L}) “orbital” angular momentum associated with the relative electron motion and internal “isospin” angular momentum (\hat{I}) associated with the atomic electron states.

As electrons that form Cooper pairs hop between sites on the lattice, they exchange $\pm 2\hbar$ units of angular momentum between the orbital and isospin angular momentum. These “isospin-flip” hopping processes are the analogue of the spin-orbit coupling terms in metals which give rise to Rashba coupling terms. We write down the tight-binding two-orbital Hamiltonian $H_0(\mathbf{k})$ for the electron motion⁴⁴ in a fashion that highlights the isospin-orbital Rashba coupling,

$$\hat{H}_0(\mathbf{k}) = \epsilon_s(\mathbf{k})\mathbf{1} - \vec{B}_{\mathbf{k}} \cdot \vec{I}. \quad (1)$$

Here we have introduced a triplet of isospin Pauli matrices $\vec{I} = (I_1, I_2, I_3)$ which span the orbital space, defined as $I_1 \equiv |xz\rangle\langle yz| + |yz\rangle\langle xz|$, $I_2 \equiv -i|xz\rangle\langle yz| + i|yz\rangle\langle xz|$ and $I_3 \equiv |xz\rangle\langle xz| - |yz\rangle\langle yz|$.

$|zy\rangle\langle zy|$. The orbital Rashba field $\vec{B}_{\mathbf{k}} = (\epsilon_{xy}(\mathbf{k}), 0, \epsilon_{x^2-y^2}(\mathbf{k})) = B_{\mathbf{k}} \hat{\mathbf{n}}_{\mathbf{k}}$ has magnitude $B_{\mathbf{k}} = \sqrt{\epsilon_{x^2-y^2}(\mathbf{k})^2 + \epsilon_{xy}(\mathbf{k})^2}$ and direction $\hat{\mathbf{n}}_{\mathbf{k}} = (\sin \phi_{\mathbf{k}}, 0, \cos \phi_{\mathbf{k}})$ where $\phi_{\mathbf{k}} = \tan^{-1}(\epsilon_{xy}(\mathbf{k})/\epsilon_{x^2-y^2}(\mathbf{k}))$ is the clockwise angle of rotation about the \hat{y} axis. The transformation behavior of the first and third components of $\hat{\mathbf{n}}_{\mathbf{k}}$ is dictated by the point group transformation, while the vanishing second component of $\hat{\mathbf{n}}_{\mathbf{k}}$ is a consequence of time reversal symmetry. Electron hopping between iron atoms proceeds predominantly via the arsenic atoms, resulting in a preferential hopping of yz -orbitals along the x axis and xz -orbitals along the y axis. The corresponding tight-binding description⁴⁴ then gives $\epsilon_s(\mathbf{k}) = 4t_2(c_x c_y) + 2t_1(c_x + c_y)$, $\epsilon_{xy}(\mathbf{k}) = 4t_4 s_x s_y$ and $\epsilon_{x^2-y^2}(\mathbf{k}) = 2t_3(c_x - c_y)$.

It is straightforward to diagonalize the Hamiltonian to obtain two quasi-particle bands of opposite helicities, $I = \pm 1$, where I is the eigenvalue of the “helicity” operator $\vec{I} \cdot \hat{\mathbf{n}}_{\mathbf{k}}$. The energies are given by $E_I(\mathbf{k}) = \epsilon_s(\mathbf{k}) - \text{sgn}(I)B_{\mathbf{k}}$, giving rise to a normal state Hamiltonian

$$H_0 = \sum_{\mathbf{k}, \sigma} (E_+(\mathbf{k}) a_{\mathbf{k}\sigma}^\dagger a_{\mathbf{k}\sigma} + E_-(\mathbf{k}) b_{\mathbf{k}\sigma}^\dagger b_{\mathbf{k}\sigma}) \quad (2)$$

where

$$\begin{aligned} a_{\mathbf{k}, \sigma}^\dagger &= u_{\mathbf{k}} c_{\mathbf{k}, xz, \sigma}^\dagger + v_{\mathbf{k}} c_{\mathbf{k}, yz, \sigma}^\dagger, \\ b_{\mathbf{k}, \sigma}^\dagger &= u_{\mathbf{k}} c_{\mathbf{k}, yz, \sigma}^\dagger - v_{\mathbf{k}} c_{\mathbf{k}, xz, \sigma}^\dagger \end{aligned} \quad (3)$$

are the hole and electron quasi-particle creation operators respectively. The helicity has an “ s^\pm ” symmetry, with $I = +1$ on the hole pockets and $I = -1$ on the electron pockets. The quasi-particle coherence factors $(u_{\mathbf{k}}, v_{\mathbf{k}}) = (\cos \phi_{\mathbf{k}}/2, \sin \phi_{\mathbf{k}}/2)$ are determined by the orientation of the $\hat{\mathbf{n}}_{\mathbf{k}}$ vector, which winds twice in isospin space as one passes around the Γ point (see Fig. 1). The vector $\vec{n}_{\mathbf{k}}$ reverses its direction of rotation around the (π, π) point, and when this hole pocket is

translated into the central zone, it forms a second Γ pocket with an opposite orbital character to the first.

The multi-orbital nature of the band structure suggests that the gap function is entangled with the orbital isospin. To this end we make the ansatz that the s^\pm gap alternates between the electron and hole pocket, but is constant on each of these Fermi surfaces, given by a pairing Hamiltonian

$$H_{sc} = \Delta \sum_{\mathbf{k}} \left[a_{\mathbf{k}\uparrow}^\dagger a_{-\mathbf{k}\downarrow}^\dagger - b_{\mathbf{k}\downarrow}^\dagger b_{-\mathbf{k}\uparrow}^\dagger + \text{H.c.} \right], \quad (4)$$

where for simplicity, we have chosen the two gaps to be of equal magnitude. In a conventional picture of s^\pm pairing, the gap function $\Delta^\pm(\mathbf{k}) \sim \Delta_0 \cos(k_x) \cos(k_y)$ on all bands. As we now show, in this alternative interpretation of s^\pm pairing, a condensate of orbitally entangled d-wave pairs hides behind the topologically non-trivial band structure.

The orbital Rashba field $\hat{n}_{\mathbf{k}}$ shown in Fig. 1, defines a quasiparticle reference frame which rotates in orbital space as it moves through momentum space. Though the s^\pm gap is constant in the quasiparticle reference frame, when transformed back into the stationary orbital reference frame, a non-trivial orbital and isospin structure is revealed. Using equations (3), carrying out the transformation back into the fixed atomic orbital basis, we obtain

$$\begin{aligned} H_{sc} &= -\Delta \sum_{\mathbf{k}} c_{\mathbf{k}\uparrow}^\dagger \left[(u_{\mathbf{k}}^2 - v_{\mathbf{k}}^2) I_3 + 2u_{\mathbf{k}}v_{\mathbf{k}} I_1 \right] c_{-\mathbf{k}\downarrow}^\dagger \\ &= \frac{1}{2} \sum_{\mathbf{k}} c_{\mathbf{k}}^\dagger \left[(\Delta_{x^2-y^2}(\mathbf{k}) I_3 + \Delta_{xy}(\mathbf{k}) I_1 \right] i\sigma_2 c_{-\mathbf{k}}^\dagger \end{aligned} \quad (5)$$

where we have used the fact that $u_{\mathbf{k}}$ and $v_{\mathbf{k}}$ are odd functions of momentum. Here $\Delta_{xy}(\mathbf{k}) = -\frac{\Delta}{|B_{\mathbf{k}}|} \epsilon_{xy}(\mathbf{k})$ and $\Delta_{x^2-y^2}(\mathbf{k}) = -\frac{\Delta}{|B_{\mathbf{k}}|} \epsilon_{x^2-y^2}(\mathbf{k})$ define d-wave form-factors. In this way, the gap

function is revealed to be a triplet pair wavefunction, reminiscent of superfluid He-3B, except that it involves isospin rather than spin operators, and the gap functions have d-wave rather than p-wave form-factors. This leads us to identify the s^\pm gap as a “d-wave orbital triplet”⁴⁵ condensate.

To further elucidate the orbital triplet condensate, we combine $H_0 + H_{sc}$ to obtain

$$H = \frac{1}{2} \sum_{\mathbf{k}} \psi_{\mathbf{k}}^\dagger [(\epsilon_s(\mathbf{k}) - \vec{B}_{\mathbf{k}} \cdot \vec{I})\gamma_3 + \vec{d}_{\mathbf{k}} \cdot \vec{I}\gamma_1] \psi_{\mathbf{k}}, \quad (6)$$

where we have used a four-component Balian Werthammer²⁵ notation, $\psi_{\mathbf{k}}^\dagger = (c_{\mathbf{k}I\sigma}^\dagger, c_{-\mathbf{k}I\sigma'}^\dagger(i\sigma_2)_{\sigma'\sigma})$, using I and σ denote the orbital and spin quantum numbers and $\vec{\gamma} = (\gamma_1, \gamma_2, \gamma_3)$ for the 2×2 Nambu matrices acting in particle-hole space. The Bogoliubov spectrum is then given by,

$$E^\alpha(\mathbf{k}) = \left[(\epsilon_{\mathbf{k}}^2 + |\vec{B}_{\mathbf{k}}|^2 + |\vec{d}_{\mathbf{k}}|^2) - \alpha \sqrt{4\epsilon_{\mathbf{k}}^2 |\vec{B}_{\mathbf{k}}|^2 + 4|\vec{B}_{\mathbf{k}} \times \vec{d}_{\mathbf{k}}|^2} \right]^{1/2} \quad (7)$$

where, in analogy to $^3\text{He-B}$, we have defined a \vec{d} -vector for the orbital triplet pairing,

$$\vec{d}_{\mathbf{k}} = (\Delta_{xy}, 0, \Delta_{x^2-y^2}), \quad (8)$$

Like the orbital Rashba vector $\vec{B}_{\mathbf{k}}$, the \vec{d} -vector precesses in the x-z plane of isospin space, its d-wave form factor guaranteeing that it rotates twice as \mathbf{k} goes around the Γ point. The vanishing second component of \vec{d} is a consequence of time reversal symmetry of the pairing state. As long as there is no relative motion between $\vec{B}_{\mathbf{k}}$ and $\vec{d}_{\mathbf{k}}$, the gap function preserves its phase and the underlying nodes of the d-wave form factor are “hidden”. This superconductor, in which the two d-wave condensates are locked in phase, is normally favored by its large isotropic gap, and corresponds to a low spin ($J = L - I = 2 - 2 = 0$) s^\pm condensate. We note as an aside that were $^3\text{He-B}$ to contain an analogous spin Rashba term, its Fermi surface would also split into two components with an s^\pm structure⁴⁶.

Our picture allows us to consider generalizations in which the relative sign of the two d-wave components is reversed. We will show that in the case where the electron or hole Fermi pockets are uncompensated, the Coulomb interaction changes the sign of the Josephson coupling between the two condensates, driving this reversal. When the two condensates have opposite phase, $\vec{d}_{\mathbf{k}}$ rotates oppositely to $\vec{n}_{\mathbf{k}}$, and since each vector counter rotates twice passing around the Γ point, in the quasiparticle reference frame the relative phase between the two vectors rotates four times as one passes around the Γ point, giving rise to a “high spin” gap function with g-wave $J = L + I = 4$ total angular momentum and an octet gap structure. To reveal the octet gap structure, we reverse the sign of $\Delta_{x^2-y^2}$ in Eq. 5 and transforming back to the quasiparticle basis, to obtain

$$\begin{aligned}
H_1 &= \sum_{\mathbf{k}} c_{\mathbf{k}}^{\dagger} [\Delta_{xy} I_1 - \Delta_{x^2-y^2} I_3] (i\sigma_2) c_{-\mathbf{k}}^{\dagger} + \text{H.C.} \\
&= -\frac{1}{B_{\mathbf{k}}} (\Delta_{xy} \epsilon_{xy} - \Delta_{x^2-y^2} \epsilon_{x^2-y^2}) \left[a_{\mathbf{k}\uparrow}^{\dagger} a_{-\mathbf{k}\downarrow}^{\dagger} - b_{\mathbf{k}\uparrow}^{\dagger} b_{-\mathbf{k}\downarrow}^{\dagger} \right] \\
&\quad - \frac{1}{B_{\mathbf{k}}} (\Delta_{xy} \epsilon_{x^2-y^2} + \Delta_{x^2-y^2} \epsilon_{xy}) \left[a_{\mathbf{k}\uparrow}^{\dagger} b_{-\mathbf{k}\downarrow}^{\dagger} - b_{\mathbf{k}\uparrow}^{\dagger} a_{-\mathbf{k}\downarrow}^{\dagger} \right] + \text{H.C}
\end{aligned} \tag{9}$$

The octet gap symmetry is revealed by setting $\Delta_{xy}(\mathbf{k}) \sim \epsilon_{xy}$ and $\Delta_{x^2-y^2}(\mathbf{k}) \sim \epsilon_{x^2-y^2}$, for which the band-diagonal component of the pairing is given by $\Delta(\mathbf{k}) \propto (\epsilon_{xy}^2 - \epsilon_{x^2-y^2}^2) \sim \cos(4\theta)$, corresponding to a gap with eight nodes whose exact positions are determined by the ratio of gap magnitudes Δ_2/Δ_1 . There is also an inter-band A_{2g} pairing term, given by $\vec{B}_{\mathbf{k}} \times \vec{d}_{\mathbf{k}} \propto (\Delta_{xy} \epsilon_{x^2-y^2} - \Delta_{x^2-y^2} \epsilon_{xy})$ which produces a small second-order correction to the gap which does not alter its basic symmetry.

The internal d -wave structure of the orbital triplet will always act to minimize the total Coulomb repulsion; however, the orbital Rashba terms will in general mix the d -wave orbital triplet

pairing with conventional s^{++} pairing. In electron-hole pocket materials, the phase cancellation of the electron and hole pockets (and opposite helicities) minimizes the on-site s -wave component induced by the orbital Rashba terms in the kinetic energy, thereby minimizing the on-site Coulomb repulsion at iron sites. However, in systems with just electron or hole pockets, this cancellation fails. In this situation we expect the orbital triplets to accommodate the Coulomb interaction by reversing the helicity of the \vec{d} vector, building explicit octet nodes into the gap function.

Fig. 2 shows the octet superconducting gap around the hole pockets around Γ for the high angular momentum case. Recent ARPES experiments on KFe_2As_2 show evidence for the high angular momentum octet superconducting state on the hole pockets¹, which is confirmed to have nodes via thermal conductivity measurements². Our orbital triplet scenario is consistent with these observations. Fig. 2 shows the gap in the vicinity of the electron pockets around M . Orbital triplet pairing also reproduces the large isotropic gap seen experimentally in strongly electron doped materials, where generically, the octet line nodes do not intersect the electron pockets, leading to a full gap.

We now discuss the nature of the phase transition between the low-spin s^\pm and the high spin octet state. The basic structure of the phase transition can be modeled using a Landau Free energy, which we write as $F = F_{DOT} + F_S$, where

$$\begin{aligned}
F_{DOT} &= \alpha(T - T_c)(|\Delta_1|^2 + |\Delta_2|^2) - \chi_{12}\Delta_1\Delta_2 + \beta_1(|\Delta_1|^4 + |\Delta_2|^4) + \beta_2|\Delta_1|^2|\Delta_2|^2 \\
F_S &= U|\Delta_s|^2 - \chi_{1s}\Delta_1\Delta_s - \chi_{2s}\Delta_2\Delta_s + \beta_3|\Delta_s|^4.
\end{aligned} \tag{10}$$

F_{DOT} describes the energetics of the d-wave orbital triplet pairing, where Δ_1 and Δ_2 denote the

order parameters of the two d-wave condensates: for example, $\Delta_{xy} = \Delta_1 s_x s_y$ and $\Delta_{x^2-y^2} = \Delta_1(c_x - c_y)$. The term χ_{12} describes the attractive Josephson coupling between the two gap functions generated by the orbital Rashba effect, which will tend to phase-lock the two condensates to produce a fully gapped s^\pm state. A microscopic calculation gives $\chi_{12} = (N(0)/4) \ln(\frac{\omega_{sf}}{2\pi T})$ (see SOM) where $N(0)$ is the density of states and ω_{sf} is the characteristic cut-off energy scale of the d-wave pairing.

F_S describes the effect of the Coulomb interaction, which imposes an energy cost U associated with any uniform s-wave order parameter. The orbital-Rashba coupling generates a linear coupling between the d- and s-wave condensates described by χ_{1s} and χ_{2s} . For small values of Δ_s , the s-wave term can be integrated out, yielding a renormalized Josephson coupling

$$\chi_{12} \rightarrow \chi_{12}^{eff} = \chi_{12} - \left(\frac{\chi_{1s}\chi_{2s}}{U} \right) \quad (11)$$

A microscopic calculation shows that $\chi_{1s} = \chi_{2s} \sim \sum_{I=\pm} \text{sgn}(I) \ln(\frac{\omega_{sf}}{2\pi T})$, with equal and opposite contributions from the two helical bands. When both bands cross E_F , $\chi_{1s} = \chi_{2s} = 0$, thereby demonstrating the phase cancelation mechanism; in this case the Josephson coupling thus $\chi_{12}^{eff} > 0$, driving the system into the energetically favored s^\pm state. However, this compensation fails when the electron band is doped away from E_F , and $\chi_{1s} = \chi_{2s} \sim -(N(0)/2) \ln(\frac{\omega_{sf}}{2\pi T})$. At this Lifshitz point, the Coulomb repulsion renormalizes the Josephson forcing it to change sign, and a first-order phase transition from the s^\pm to the octet state will occur. A microscopic calculation

gives (see online material)

$$\chi_{12}^{eff} = N(0) \ln \left(\frac{\omega_{sf}}{2\pi T_c} \right) \times \begin{cases} \frac{1}{4} & \text{(electron and hole pockets),} \\ -\frac{1}{8} & \text{(hole pockets only).} \end{cases} \quad (12)$$

We thus expect a quantum phase transition from the low angular momentum s^\pm superconducting state to the high angular momentum state when the Coulomb repulsion overcomes the internal Josephson coupling. This is most likely to occur in systems without electron pockets. KFe_2As_2 exhibits exactly such a Fermi surface structure, and experiments on this material show that it undergoes a first order transition under pressure from a gapless to a fully gapped superconductor². This transition has been interpreted as a competition between two fine-tuned d-wave and s-wave pairing mechanisms². However, the high to low spin transition of the condensate provides an alternative way to account for this transition within a single pairing mechanism.

One of the ways in which the orbital entanglement of the condensate can be measured, is using polarized Angle Resolved Photoelectron Spectroscopy (pARPES), which has been recently used to measure the orbital character of the surface states in the topological insulator, Bi_2Se_3 ⁴⁷. As the orbitally entangled condensate develops, we predict that orbital anisotropy of the ARPES signal will change in a very specific fashion. Polarization dependent ARPES techniques determine the momentum-resolved orbital anisotropy of the quasiparticles, defined by $I_3(\mathbf{k}) = n_{xz}(\mathbf{k}) - n_{yz}(\mathbf{k})$. In the superconducting state, Andreev scattering off the orbitally entangled pairs modifies the orbital Rashba field. This is because Andreev scattering off the orbitally entangled condensate contains an interband term of strength proportional to $\vec{d}_{\mathbf{k}} \times \vec{B}_{\mathbf{k}}$, so that two successive successive Andreev scattering events give rise to an additional component to the orbital Rashba field. A

detailed calculation of the resulting orbital anisotropy (see Supplementary Information for details) gives

$$\delta I_3(\mathbf{k}) = I_3^{sc} - I_3^n \approx \frac{\Delta_{xy}(\mathbf{k}) (\epsilon_{x^2-y^2}(\mathbf{k}) \Delta_{xy}(\mathbf{k}) - \epsilon_{xy}(\mathbf{k}) \Delta_{x^2-y^2}(\mathbf{k}))}{|\vec{B}_{\mathbf{k}}|^2 \Delta_{sc}(\mathbf{k})} \quad (13)$$

where $\Delta_{sc}(\mathbf{k})$ is the full superconducting gap. The qualitative angular form of this function is $\delta I_3(\theta) \sim \sin(2\theta) \sin(4\theta) \sim \cos(6\theta)$. The overall magnitude is proportional to $1/\Delta_{sc}(\mathbf{k})$, so that the changes in the orbital character are expected to be greatly enhanced in the octet state. Fig 3 contrasts the predicted orbital anisotropy for the s^\pm and octet superconductors. The vanishing of the gap in the octet state leads to a characteristic cusp like structure in the orbital anisotropy near the gap nodes, observation of which would provide a definitive test of our theory.

One of the interesting aspects of the orbital triplet condensates involves their internal topology. The unit $\hat{d}_{\mathbf{k}} = \vec{d}_{\mathbf{k}}/|d_{\mathbf{k}}|$ vector defines a winding number,

$$\oint_{\Gamma} \hat{z} \cdot \left(\hat{d}^\dagger(\mathbf{k}) \times \partial_a \hat{d}(\mathbf{k}) \right) dk_a = 2\pi\nu \quad (14)$$

The low-spin s^\pm state and high-spin octet state have opposite winding numbers $\nu = +2$ and $\nu = -2$ respectively. At an interface between these two phases, the change in topology is expected to produce gapless Andreev bound-states, loosely analogous to the Majorana surface states in $^3\text{He-B}$ ^{48–50}. However, here spin singlet character of the condensates will produce a Kramers doublet of counter-propagating Andreev bound states. This prediction could be tested using an epitaxially grown interface between optimally doped and electron or hole-doped samples.

We end by mentioning the effect of including the additional xy orbitals, neglected in our initial model of orbital triplet pairing. To describe the additional entanglement of these orbitals

with the condensate we must introduce two new orbital isospin operators $I_4 = i(|xz\rangle\langle xy| - |xy\rangle\langle xz|)$ and $I_5 = i(|yz\rangle\langle xy| - |xy\rangle\langle yz|)$. Since these operators involve a change in angular momentum of one unit, they carry internal angular momentum $I = 1$ and to form the s^\pm condensate with net angular momentum $J = L + I = 0$ their corresponding form factors must have $L = 1$ p -wave symmetry, so that now

$$H^{sc} = \sum_{\mathbf{k}} \psi_{\mathbf{k},I\sigma}^\dagger (\Delta_{xy} I_1 + \Delta_{x^2-y^2} I_3 + \Delta_x I_4 + \Delta_y I_5) \gamma_1 \psi_{\mathbf{k},I\sigma} \quad (15)$$

where $\Delta_x = \Delta \sin k_x$ and $\Delta_y = \Delta \sin k_y$. These extra terms may promote additional low-to-high spin transitions into gapless $J = I + L = 2$ d-wave states.

In conclusion, we have proposed that the s^\pm pairing in the iron based superconductors derives from an underlying orbital triplet condensate. Our model allows for the possibility of both “low” and “high” spin configurations of the orbital triplet pairs and predicts the development of a distinct orbital anisotropy signature in the ARPES spectroscopy in the superconducting phase. We note that this pairing mechanism may also be relevant for other multi-orbital superconductors such as SrRu_2O_4 .

1. Okazaki, K. et al. Octet-Line Node Structure of Superconducting Order Parameter in KFe_2As_2 . Science **337**, 1314–1317 (2012).
2. Tafti, F. F. et al. Sudden reversal in the pressure dependence of T_c in the iron-based superconductor KFe_2As_2 . NATURE PHYSICS **9**, 349–352 (2013).
3. Terasaki, N. et al. Spin Fluctuations and Unconventional Superconductivity in the Fe-Based Oxypnictide Superconductor $\text{LaFeAsO}_{0.7}$ Probed by Fe-57-NMR. J. Phys. Soc. Jpn. **78**, 013701 (2009).
4. Yashima, M. et al. Strong-Coupling Spin-Singlet Superconductivity with Multiple Full Gaps in Hole-Doped $\text{Ba}_{0.6}\text{K}_{0.4}\text{Fe}_2\text{As}_2$ Probed by Fe-57-NMR. J. Phys. Soc. Jpn. **78**, 103702 (2009).
5. Hashimoto, K. et al. Microwave Surface-Impedance Measurements of the Magnetic Penetration Depth in Single Crystal $\text{Ba}_{1-x}\text{K}_x\text{Fe}_2\text{As}_2$ Superconductors: Evidence for a Disorder-Dependent Superfluid Density. Phys. Rev. Lett. **102**, 207001 (2009).
6. Hicks, C. W. et al. Limits on the Superconducting Order Parameter in $\text{NdFeAsO}_{1-x}\text{F}_y$ from Scanning SQUID Microscopy. J. Phys. Soc. Jpn. **78**, 013708 (2009).
7. Mazin, I. I. & Schmalian, J. Pairing symmetry and pairing state in ferropnictides: theoretical overview. Physica C **469**, 614 (2009).
8. Zhang, X. et al. Observation of the Josephson Effect in $\text{Pb}/\text{Ba}_{1-x}\text{K}_x\text{Fe}_2\text{As}_2$ Single Crystal Junctions. Phys. Rev. Lett. **102**, 147002 (2009).

9. Chen, C.-T., Tsuei, C. C., Ketchen, M. B., Ren, Z.-A. & Zhao, Z. X. Integer and half-integer flux-quantum transitions in a niobium-iron pnictide loop. Nat. Phys. **6**, 260 (2010).
10. Hanaguri, T., Niitaka, S., Kuroki, K. & Takagi, H. Superconductivity in Fe(Se,Te). Science **328**, 474 (2010).
11. Hirschfeld, P. J., Korshunov, M. M. & Mazin, I. I. Gap symmetry and structure of fe-based superconductors. Rep. Prog. Phys. **74**, 124508 (2011).
12. Luan, L. et al. Local Measurement of the Superfluid Density in the Pnictide Superconductor $\text{Ba}(\text{Fe}_{1-x}\text{Co}_x)_2\text{As}_2$ across the Superconducting Dome. Phys. Rev. Lett. **106**, 067001 (2011).
13. Hoffman, J. E. Spectroscopic scanning tunneling microscopy insights into Fe-based superconductors. Rep. Prog. Phys. **74**, 124513 (2011).
14. Allan, M. P. et al. Anisotropic Energy Gaps of Iron-Based Superconductivity from Intraband Quasiparticle Interference in LiFeAs. Science **336**, 563 (2012).
15. Wang, X.-P. et al. Observation of an isotropic superconducting gap at the Brillouin zone centre of $\text{Tl}_{0.63}\text{K}_{0.37}\text{Fe}_{1.78}\text{Se}_2$. Europhys. Lett. **99**, 67001 (2012).
16. Bourbonnais, C. & Jerome, D. "Interacting electrons in quasi one dimensional organic superconductors". In Lebed, A. G. (ed.) "The Physics of Organic Superconductors and Conductors", vol. 110, 357–412 (Springer, Heidelberg, 2008).

17. Lefebvre, S. et al. Mott Transition, Antiferromagnetism, and Unconventional Superconductivity in Layered Organic Superconductors. Phys. Rev. Lett. **85**, 5420 (2000).
18. Pfleiderer, C. Superconducting phases of f -electron compounds. Rev. Mod. Phys. **81**, 1551 (2009).
19. Tsuei, C. C. & Kirtley, J. R. Phase-Sensitive Evidence for d -Wave Pairing Symmetry in Electron-Doped Cuprate Superconductors. Phys. Rev. Lett. **85**, 182 (2000).
20. Mackenzie, A. P. & Maeno, Y. The superconductivity of Sr_2RuO_4 and the physics of spin-triplet pairing. Rev. Mod. Phys. **75**, 657 (2003).
21. Rice, T. M. & Sigrist, M. Sr_2RuO_4 : an electronic analogue of He-3B. J. Phys: Cond Matter **7**, L643 (1995).
22. Ishida, K. et al. Spin-triplet superconductivity in Sr_2RuO_4 identified by ^{17}O Knight shift. Nature **396**, 658–660 (1998).
23. Luke, G. M. et al. Time-reversal symmetry-breaking superconductivity in Sr_2RuO_4 . Nature **394**, 558–561 (1998).
24. Mackenzie, A. P. & Maeno, Y. The superconductivity of Sr_2RuO_4 and the physics of spin-triplet pairing. Rev. Mod. Phys. **75**, 657–712 (2003).
25. Balian, R. & Werthamer, N. R. Superconductivity with Pairs in a Relative p-Wave. Phys. Rev. **131**, 1553–1564 (1963).

26. Anderson, P. W. & Morel, P. Generalized Bardeen-Cooper-Schrieffer States and the Proposed Low-Temperature Phase of Liquid He3. Phys. Rev. **123**, 1911–1934 (1961).
27. Osheroff, D. D. Superfluidity in ^3He : Discovery and understanding. Rev. Mod. Phys. **69**, 667–682 (1997).
28. Leggett, A. J. A theoretical description of the new phases of liquid He3. Rev. Mod. Phys. **47**, 331–414 (1975).
29. Wheatley, J. C. Experimental properties of superfluid He3. Rev. Mod. Phys. **47**, 415–470 (1975).
30. Vollhardt, D. & Wölfle, P. The Superfluid Phases of Helium 3 (Dover Publications, UK, 2013).
31. Abdel-Hafiez, M. et al. Evidence of d-wave superconductivity in $\text{K}_{1-x}\text{Na}_x\text{Fe}_2\text{As}_2$ ($x=0,0.1$) single crystals from low-temperature specific-heat measurements. Phys. Rev. B **87**, 180507 (2013).
32. Watanabe, D. et al. Doping evolution of the quasiparticle excitations in heavily hole-doped $\text{Ba}_{1-x}\text{K}_x\text{Fe}_2\text{As}_2$: A possible superconducting gap with sign-reversal between hole pockets. Phys. Rev. B **89**, 115112 (2014).
33. Okazaki, K. et al. Evidence for a $\cos(4\varphi)$ Modulation of the Superconducting Energy Gap of Optimally Doped $\text{FeTe}_{0.6}\text{Se}_{0.4}$ Single Crystals Using Laser Angle-Resolved Photoemission Spectroscopy. Phys. Rev. Lett. **109**, 237011 (2012).

34. Xu, N. et al. Possible nodal superconducting gap and Lifshitz transition in heavily hole-doped Ba_{0.1}K_{0.9}Fe₂As₂. Phys. Rev. B **88**, 220508 (2013).
35. Ota, Y. et al. Evidence for excluding the possibility of *d*-wave superconducting-gap symmetry in Ba-doped KFe₂As₂. Phys. Rev. B **89**, 081103 (2014).
36. Kittaka, S. et al. Thermodynamic Study of Nodal Structure and Multiband Superconductivity of KFe₂As₂. Journal of the Physical Society of Japan **83**, 013704 (2014).
37. Ran, Y., Wang, F., Zhai, H., Vishwanath, A. & Lee, D.-H. Nodal spin density wave and band topology of the FeAs-based materials. Phys. Rev. B **79**, 014505 (2009).
38. Yin, Z. P., Haule, K. & Kotliar, G. Kinetic frustration and the nature of the magnetic and paramagnetic states in iron pnictides and iron chalcogenides. NATURE MATERIALS **10**, 932–935 (2011).
39. Zhang, Y. et al. Orbital characters of bands in the iron-based superconductor BaFe_{1.85}Co_{0.15}As₂. Phys. Rev. B **83**, 054510 (2011).
40. Xia, Y. et al. Fermi Surface Topology and Low-Lying Quasiparticle Dynamics of Parent Fe_{1+x}Te/Se Superconductor. Phys. Rev. Lett. **103**, 037002 (2009).
41. Richard, P. et al. Observation of Dirac Cone Electronic Dispersion in BaFe₂As₂. Phys. Rev. Lett. **104**, 137001 (2010).
42. Hsieh, D. et al. Experimental determination of the microscopic origin of magnetism in parent iron pnictides (2009). 0812.2289.

43. Lee, P. & Wen, X.-G. Spin-triplet p-wave pairing in a three-orbital model for iron pnictide superconductors. Physical Review B **78**, 144517 (2008).
44. Raghu, S., Qi, X. L., Liu, C. X., Scalapino, D. J. & Zhang, S. C. Phys. Rev. B 77, 220503(R) (2008) - Minimal two-band model of the superconducting iron oxypnictides. Physical Review B (2008).
45. Ong, T. T. & Coleman, P. Tetrahedral and Orbital Pairing: A Fully Gapped Pairing Scenario for the Iron-Based Superconductors. Phys. Rev. Lett. **111**, 217003 (2013).
46. Ong, T. T. & Coleman, P. $^3\text{He-R}$: A Topological s^\pm Superfluid with Triplet Pairing. arXiv 1402.7372 (2014).
47. Cao, Y. et al. Mapping the orbital wavefunction of the surface states in three-dimensional topological insulators. NATURE PHYSICS **9**, 499–504 (2013).
48. Volovik, G. E. The Universe in a Helium Droplet (Clarendon Press, UK, 2003).
49. Volovik, G. Fermion zero modes at the boundary of superfluid $^3\text{He-B}$. JETP Letters **90**, 398–401 (2009).
50. Volovik, G. Topological invariant for superfluid $^3\text{He-B}$ and quantum phase transitions. JETP Letters **90**, 587–591 (2009).

Supplementary information is linked to the online version of the paper at www.nature.com/nature.

Acknowledgements: We should particularly like to thank Leni Boscones, Andrey Chubukov, Gabriel Kotliar, Andrew Millis, Peter Orth and Qimiao Si for discussions related to this work. We are particularly grateful to Daniel Dessau for helpful discussions on changes to the orbital character in the superconducting state. We acknowledge funding from DOE grant DE-FG02-99ER45790 (Coleman, Ong), Deutsche Forschungsgemeinschaft through DFG-SPP 1458 ‘Hochtemperatursupraleitung in Eisenpniktiden (Schmalian) and grant NSF 1066293 (Coleman) while at the Aspen Center for Physics.

Contributions The authors, T. Tzen Ong, Piers Coleman and Joerg Schmalian contributed equally in the discussions and development of the ideas in this paper. T. Tzen Ong carried out the numerical calculations of the gap and the orbital anisotropy signal in ARPES spectroscopy. All authors contributed towards the writing of the paper and supplementary materials.

Competing Interests The authors declare that they have no competing financial interests.

Correspondence and requests for materials should be addressed to Piers Coleman. (email: coleman@physics.rutgers.edu).

Figure Captions

Fig. 1. Orbital helicity and orbital triplet s^\pm superconducting state. Fig. (a) shows the orbital Rashba vector, \vec{n}_k and the orbital character in a simplified two band model for the iron-based superconductors, in the extended zone scheme. The orbital helicity $I = \vec{I} \cdot \vec{n}_k$ is positive on central hole pockets (red: $I = +1$) and negative on electron pockets (blue: $I = -1$), thus the orbital polarization of the hole Fermi surface is parallel to \vec{n}_k (Red and blue hollow arrow denotes xz and yz respectively). Fig. (b) shows the conventional s^\pm superconducting state, and Fig. (c) shows the orbital triplet s^\pm . In conventional s^\pm , the \pm sign change is determined by the $\cos(k_x) \cos(k_y)$ form factor in k -space; in the orbital triplet state, the sign change depends on the orbital helicity ($\text{sgn}(I)$) of the bands.

Fig. 2. Superconducting gap in “high”-spin orbital triplet octet state. (a) octahedral structure of the superconducting gap on the hole pocket around Γ , when \vec{n}_k and \vec{d}_k have opposite helicities, (b) fully gapped electron pocket around M .

Fig. 3. Polar plot of orbital anisotropy in s^\pm phase and octet phase. (a) & (b) show the angular dependence (from 0 to $\frac{\pi}{2}$) of the orbital anisotropy $\delta\langle I_3 \rangle$ around the hole pocket centered at Γ for the s^\pm state and octet state respectively. The $\sin(2\theta) \sin(4\theta) \sim \cos(6\theta)$ structure (dodecagonal) is clearly revealed in both cases, and the ‘high’-spin octet state shows a unique cusp-like feature at the gapless nodal points.

Fig. 4. Helical edge states of orbital triplet pairing. Helical gapless Andreev edge states at a domain wall between a low-spin s^\pm (left) and high-spin octet (right) state.

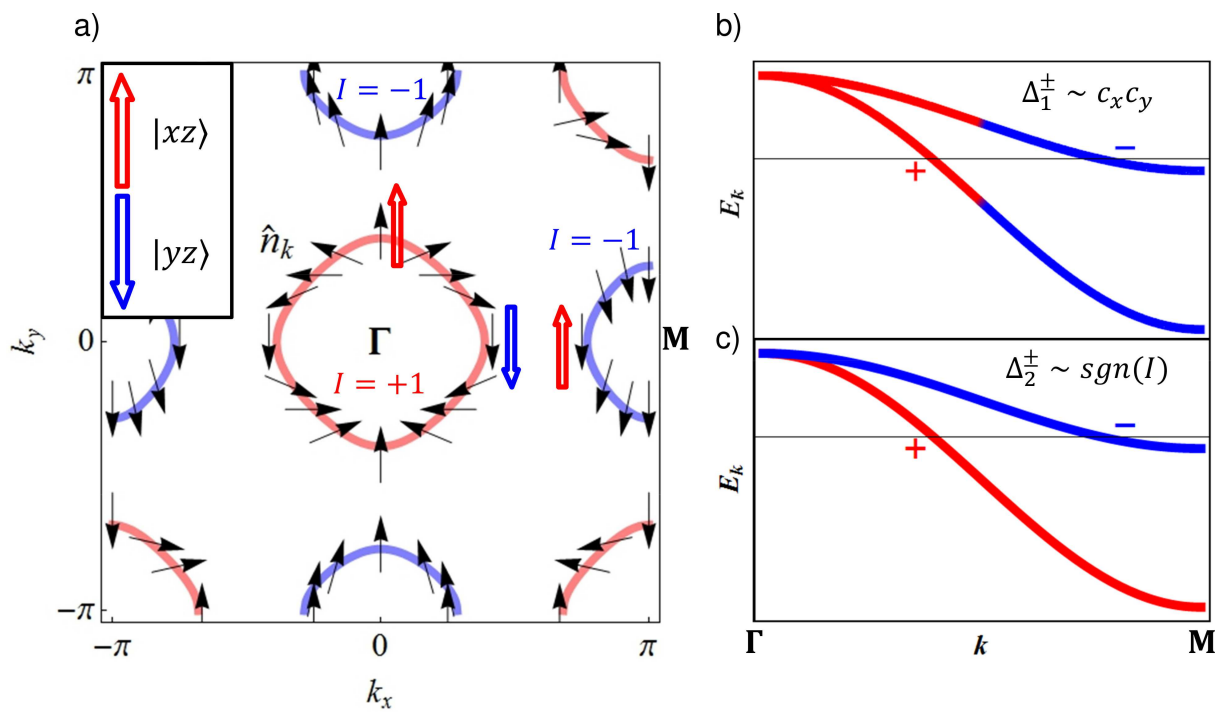


Figure 1.

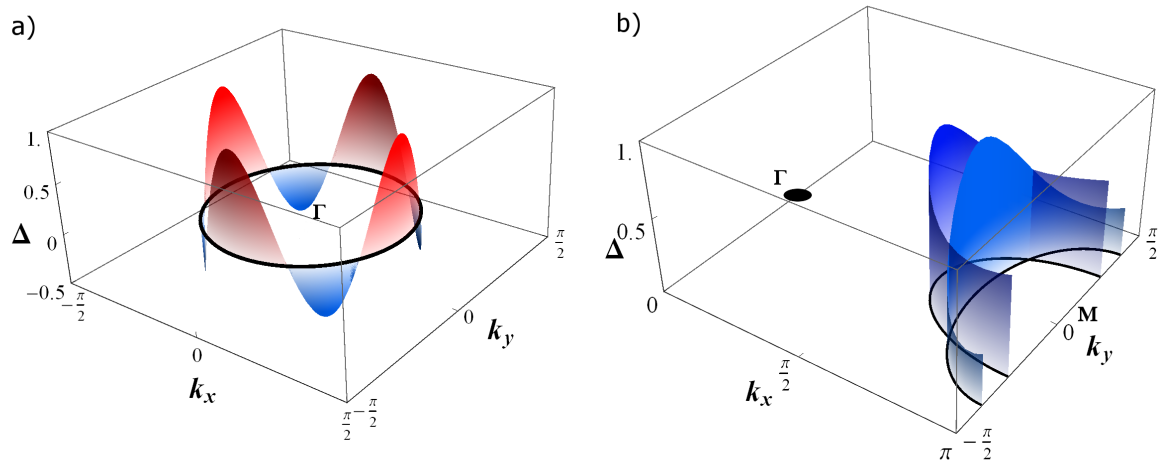


Figure 2.

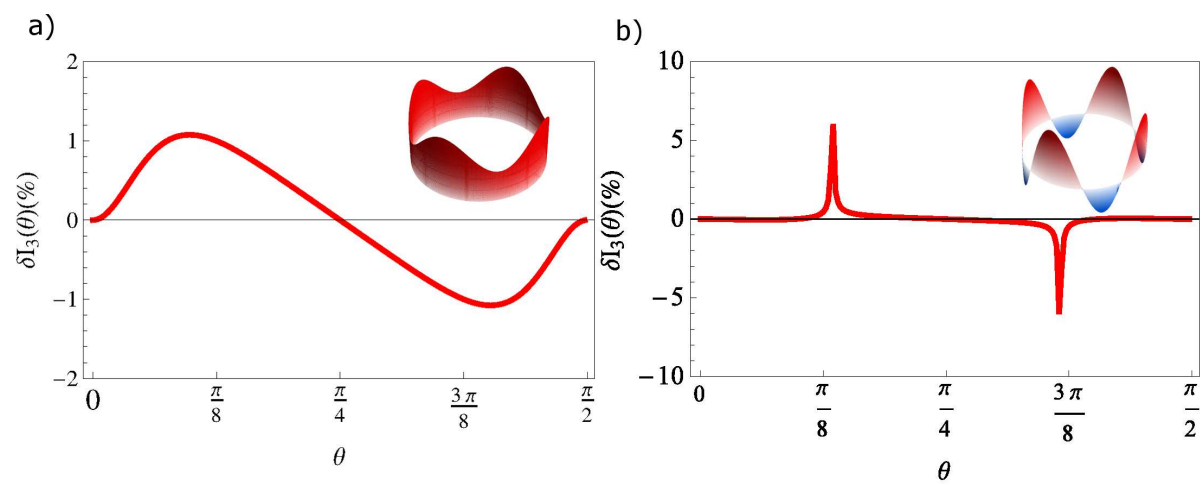


Figure 3.

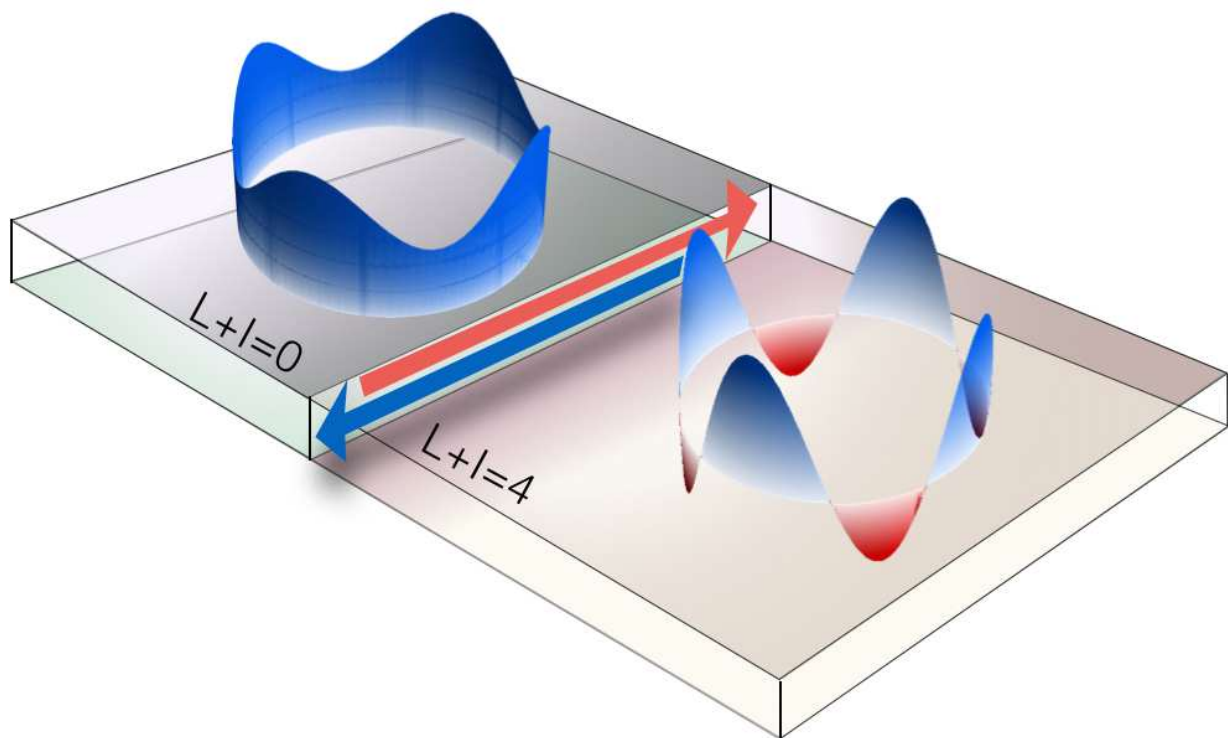


Figure 4.

Supplementary Online Material

Entangled Orbital Triplet Pairs in Iron-Based Superconductors

T. Tzen Ong ¹, P. Coleman ^{1,2} and J. Schmalian ^{3,4}

Center for Materials Theory, Rutgers University, 136 Frelinghuysen Rd., Piscataway, NJ 08854-8019, USA

²*Department of Physics, Royal Holloway, University of London, Egham, Surrey TW20 0EX, UK.*

³*Institute for Theory of Condensed Matter, Karlsruhe Institute of Technology, 76131 Karlsruhe, Germany.*

⁴*DFG Center for Functional Nanostructures, KIT, 76128 Karlsruhe, Germany.*

CONTENTS

I. Landau Free Energy & Derivation of Renormalized Josephson Coupling	2
II. Orbital Anisotropy in Superconducting Phase	6
III. Gapless Andreev Edge States	9
References	12

I. LANDAU FREE ENERGY & DERIVATION OF RENORMALIZED JOSEPHSON COUPLING

This section presents the derivation of the Landau Free energy that describes the transition between the “low”-spin s^\pm state and the “high”-spin octet state. We assume an isotropic system in Eq. (9) of the main paper to illustrate the key physics of renormalization of the Josephson coupling χ_{12} by the Coulomb repulsion; hence the coefficients for Δ_1 and Δ_2 are equal. In the physical systems with tetragonal symmetry, the coefficients for Δ_1 and Δ_2 are generally not equal as they are not related by symmetry operations of the C_{4v} group. Thus, the free energy would have the general form,

$$\begin{aligned} F &= F_{DOT} + F_s, \\ F_{DOT} &= \alpha_1(T - T_c)|\Delta_1|^2 + \alpha_2(T - T_c)|\Delta_2|^2 - \chi_{12}\Delta_1\Delta_2 \\ &\quad + \beta_1|\Delta_1|^4 + \beta_2|\Delta_2|^4 + \beta_{12}|\Delta_1|^2|\Delta_2|^2, \\ F_S &= U|\Delta_s|^2 - \chi_{1s}\Delta_1\Delta_s - \chi_{2s}\Delta_2\Delta_s + \beta_3|\Delta_s|^4. \end{aligned} \quad (1)$$

where Δ_1 and Δ_2 are the gap parameters for the d_{xy} and $d_{x^2-y^2}$ orbital triplet condensates. In the isotropic case described in the main paper, $\alpha_1 = \alpha_2$ and $\beta_1 = \beta_2$. The “low”-spin to “high”-spin transition is driven by a change in the relative orientation of $\vec{d}_{\mathbf{k}}$ with respect to $\vec{n}_{\mathbf{k}}$, i.e. by reversing $\text{sign}(\Delta_1\Delta_2)$. The relative phase of Δ_1 and Δ_2 , is determined by the internal Josephson coupling χ_{12} . When both helical bands cross E_F , we shall see that $\chi_{12} > 0$ while χ_{1s} and χ_{2s} are almost zero, so the ground-state energy is minimized when Δ_1 and Δ_2 have the same phase, forming an isotropic gap with no nodes. By contrast, when one band is removed from the Fermi surface by doping, then χ_{1s} and χ_{2s} become large, and the effective Josephson coupling becomes

$$\chi_{12}^{eff} = \chi_{12} - \frac{\chi_{1s}\chi_{2s}}{\chi_s} < 0 \quad (2)$$

causing a reversal of the relative sign of the two condensates and the formation of nodes in the gap.

We can derive the free energy using a BCS Hamiltonian that includes the orbital triplet pairing and a repulsive Hubbard U term, which we factorize into a product of s -wave pairing terms using the Hubbard-Stratonovich method,

$$H^U = U \sum_{i,I} n_{iI\uparrow} n_{iI\downarrow} \rightarrow \sum_{i,I} \Delta_s c_{i,I,\uparrow}^\dagger c_{i,I,\downarrow}^\dagger + H.C. - |\Delta_s|^2/U, \quad (3)$$

to obtain

$$H = \sum_{\mathbf{k}} \psi_{\mathbf{k}}^{\dagger} \left[\epsilon_s(\mathbf{k}) \gamma_3 + \vec{B}_{\mathbf{k}} \cdot \vec{I} + \vec{d}_{\mathbf{k}} \cdot \vec{I} \gamma_1 + \Delta_s \gamma_1 \right] \psi_{\mathbf{k}} + N_s \left(\frac{\Delta_1^2}{g_1} + \frac{\Delta_2^2}{g_2} - \frac{\Delta_s^2}{U} \right), \quad (4)$$

where N_s is the number of lattice sites and the Rashba and orbital d-vectors are defined by

$$\begin{aligned} \vec{B}_{\mathbf{k}} &= (\epsilon_{xy}, 0, \epsilon_{x^2-y^2}), \\ \vec{d}_{\mathbf{k}} &= (\Delta_{xy}, 0, \Delta_{x^2-y^2}) = (\Delta_1 d_{xy}, 0, \Delta_2 d_{x^2-y^2}), \end{aligned} \quad (5)$$

where d_{xy} and $d_{x^2-y^2}$ are d-wave form factors, for instance $d_{xy} = s_x s_y$ and $d_{x^2-y^2} = (c_x - c_y)$ in a tight binding basis.

The Bogoliubov spectrum is,

$$E^{\alpha}(\mathbf{k}) = \left[A(\mathbf{k}) - \alpha \sqrt{A^2(\mathbf{k}) - \gamma^2(\mathbf{k})} \right]^{\frac{1}{2}}, \quad (6)$$

where $\alpha = \pm 1$ for the two superconducting bands and

$$\begin{aligned} A(\mathbf{k}) &= \epsilon_s(\mathbf{k})^2 + |\vec{B}_{\mathbf{k}}|^2 + |\vec{d}_{\mathbf{k}}|^2 + \Delta_s^2, \\ \gamma(\mathbf{k})^2 &= \left[\epsilon_s(\mathbf{k})^2 - |\vec{B}_{\mathbf{k}}|^2 + |\vec{d}_{\mathbf{k}}|^2 - \Delta_s^2 \right]^2 \\ &\quad + 4 [\Delta_{xy}(\mathbf{k}) \epsilon_{xy}(\mathbf{k}) + \Delta_{x^2-y^2}(\mathbf{k}) \epsilon_{x^2-y^2}(\mathbf{k}) - \Delta_s \epsilon_s(\mathbf{k})]^2. \end{aligned} \quad (7)$$

The free energy is then given by,

$$F = N_s \left[\frac{\Delta_1^2}{g_1} + \frac{\Delta_2^2}{g_2} - \frac{\Delta_s^2}{U} \right] - 2T \sum_{\mathbf{k}, \alpha} \ln \left[2 \cosh \left(\frac{E^{\alpha}(\mathbf{k})}{2T} \right) \right]. \quad (8)$$

A Taylor expansion of Eq. 8 will then give us the coefficients of the Landau Free energy in Eq. 1. We will now carry out the calculation around the saddle point, which gives the following coupled gap equations,

$$\begin{pmatrix} \frac{1}{g_1} - \tilde{\chi}_{11} & -\tilde{\chi}_{12} & -\tilde{\chi}_{1s} \\ -\tilde{\chi}_{12} & \frac{1}{g_2} - \tilde{\chi}_{22} & -\tilde{\chi}_{2s} \\ -\tilde{\chi}_{1s} & -\tilde{\chi}_{2s} & -\frac{1}{U} - \tilde{\chi}_s \end{pmatrix} \begin{pmatrix} \Delta_1 \\ \Delta_2 \\ \Delta_s \end{pmatrix} = 0. \quad (9)$$

Denoting $\int_{\mathbf{k}} = \int \frac{d^2 k}{(2\pi)^2}$, the Josephson couplings between the different pairing channels

are then given as follows:

$$\tilde{\chi}_{11} = \sum_{\alpha=\pm 1} \int_{\mathbf{k}} \frac{\text{th}(\beta E^\alpha(\mathbf{k})/2)}{2E^\alpha(\mathbf{k})} \left[1 - 2\alpha \frac{(\epsilon_{x^2-y^2})^2 + \Delta_s^2}{\sqrt{A^2 - \gamma^2}} \right] d_{xy}^2, \quad (10)$$

$$\tilde{\chi}_{22} = \sum_{\alpha=\pm 1} \int_{\mathbf{k}} \frac{\text{th}(\beta E^\alpha(\mathbf{k})/2)}{2E^\alpha(\mathbf{k})} \left[1 - 2\alpha \frac{(\epsilon_{xy})^2 + \Delta_s^2}{\sqrt{A^2 - \gamma^2}} \right] d_{x^2-y^2}^2, \quad (11)$$

$$\tilde{\chi}_s = \sum_{\alpha=\pm 1} \int_{\mathbf{k}} \frac{\text{th}(\beta E^\alpha(\mathbf{k})/2)}{2E^\alpha(\mathbf{k})} \left[1 - 2\alpha \frac{(\Delta_{x^2-y^2})^2 + \Delta_{xy}^2}{\sqrt{A^2 - \gamma^2}} \right], \quad (12)$$

$$\tilde{\chi}_{12} = \sum_{\alpha=\pm 1} \int_{\mathbf{k}} \frac{\text{th}(\beta E^\alpha(\mathbf{k})/2)}{2E^\alpha(\mathbf{k})} \left[2\alpha \frac{\epsilon_{xy}\epsilon_{x^2-y^2}}{\sqrt{A^2 - \gamma^2}} \right] d_{xy} d_{x^2-y^2} \quad (13)$$

$$\tilde{\chi}_{1s} = - \sum_{\alpha=\pm 1} \int_{\mathbf{k}} \frac{\text{th}(\beta E^\alpha(\mathbf{k})/2)}{2E^\alpha(\mathbf{k})} \left[2\alpha \frac{\epsilon_{xy}\epsilon_s}{\sqrt{A^2 - \gamma^2}} \right] d_{xy}, \quad (14)$$

$$\tilde{\chi}_{2s} = - \sum_{\alpha=\pm 1} \int_{\mathbf{k}} \frac{\text{th}(\beta E^\alpha(\mathbf{k})/2)}{2E^\alpha(\mathbf{k})} \left[2\alpha \frac{\epsilon_{x^2-y^2}\epsilon_s}{\sqrt{A^2 - \gamma^2}} \right] d_{x^2-y^2}, \quad (15)$$

where for clarity, we have suppressed the momentum labels. Evaluating $\tilde{\chi}_{12}$, $\tilde{\chi}_{1s}$ and $\tilde{\chi}_{2s}$ at $T = T_c$ for $\Delta_1 = \Delta_2 = \Delta_s = 0$ gives the Landau free energy coefficients χ_{12} , χ_{1s} and χ_{2s} in Eq. (9) of the main paper (here we drop the tilde's to denote the evaluation of these quantities at T_c). The coefficients β_1 , β_2 and β_3 are given by Taylor expansions of $\tilde{\chi}_{12}$, $\tilde{\chi}_{1s}$ and $\tilde{\chi}_{2s}$.

$$\begin{aligned} \beta_1 &= -\frac{1}{4} \frac{\partial \tilde{\chi}_{11}}{\partial \Delta_1^2}, \\ \beta_2 &= -\frac{1}{4} \frac{\partial \tilde{\chi}_{22}}{\partial \Delta_2^2}, \\ \beta_{12} &= -\frac{1}{2} \left(\frac{\partial \tilde{\chi}_{11}}{\partial \Delta_2^2} + \frac{\partial \tilde{\chi}_{12}}{\partial \Delta_1 \Delta_2} \right). \end{aligned} \quad (16)$$

To demonstrate the renormalization of the Josephson coupling χ_{12} by the Coulomb repulsion, we solve for Δ_s in the third row of Eq. 9,

$$\Delta_s = - \left(\frac{\chi_{1s}\Delta_{1s} + \chi_{2s}\Delta_{2s}}{1/U + \chi_s} \right). \quad (17)$$

Substituting this back into the first two rows, we obtain

$$\begin{pmatrix} \frac{1}{g_1} - \chi_{11}^{eff} & -\chi_{12}^{eff} \\ -\chi_{12}^{eff} & \frac{1}{g_2} - \chi_{22}^{eff} \end{pmatrix} \begin{pmatrix} \Delta_1 \\ \Delta_2 \end{pmatrix} = 0. \quad (18)$$

where

$$\chi_{12}^{eff} = \chi_{12} - \frac{\chi_{1s}\chi_{2s}}{\chi_s}, \quad (U \rightarrow \infty), \quad (19)$$

is an effective, renormalized χ_{12}^{eff} , while

$$\begin{aligned}\chi_{11}^{eff} &= \chi_{11} - \frac{\chi_{1s}\chi_{1s}}{\chi_s}, \\ \chi_{22}^{eff} &= \chi_{22} - \frac{\chi_{2s}\chi_{2s}}{\chi_s},\end{aligned}\tag{20}$$

are the corresponding diagonal susceptibilities. Since χ_{1s} and χ_{2s} have the same sign, the Coulomb interaction thus *reduces* the Josephson coupling χ_{12} between the d-wave condensates to a smaller value χ_{12}^{eff} . The phase transition to the octet state occurs when χ_{12}^{eff} changes sign. This will occur when the system is strongly hole or electron doped, such that only hole or electron pockets survive at the Fermi surface.

To illustrate the sign change of χ_{12}^{eff} at the phase transition, we use using a simplified momentum-independent orbital Rashba coupling with $\epsilon_{xy}(\mathbf{k}) = \tilde{t} \sin(2\theta_{\mathbf{k}})$ and $\epsilon_{x^2-y^2}(\mathbf{k}) = \tilde{t} \cos(2\theta_{\mathbf{k}})$. In this case, the helical bands are split apart by \tilde{t} and have a constant density of state $N(0)$. Note that at T_c ,

$$E^\alpha(\mathbf{k}) = \left| |\epsilon_s(\mathbf{k})| - \alpha \tilde{t} \right| = |\epsilon_s(\mathbf{k}) - \alpha \operatorname{sgn}(\epsilon_s(\mathbf{k}))\tilde{t}| \equiv |\epsilon_s - I\tilde{t}| \equiv |\epsilon_I| \tag{21}$$

where we have introduced the normal-state band index

$$I = \alpha \operatorname{sgn}(\epsilon_s). \tag{22}$$

The appearance of the $\operatorname{sgn}(\epsilon_s)$ separating the normal and superconducting state band indices is important in keeping track of which susceptibilities have cancelling logarithmic components. We can then make the substitutions

$$\epsilon_I = \epsilon_s - I\tilde{t} \tag{23}$$

$$\frac{\tanh\left(\frac{\beta E^\alpha(\mathbf{k})}{2}\right)}{2E^\alpha(\mathbf{k})} = \frac{\tanh\left(\frac{\beta \epsilon_I}{2}\right)}{2\epsilon_I} \tag{24}$$

$$\frac{2\alpha}{\sqrt{A^2 - \gamma^2}} = \frac{\alpha}{|\epsilon_s|\tilde{t}} = \frac{\alpha \operatorname{sgn}(\epsilon_s)}{\epsilon_s \tilde{t}} = \frac{I}{\epsilon_s \tilde{t}} = \frac{I}{\tilde{t}(\epsilon_I + I\tilde{t})} \tag{25}$$

$$\frac{2\alpha \epsilon_s}{\sqrt{A^2 - \gamma^2}} = \frac{\alpha \epsilon_s}{|\epsilon_s|\tilde{t}} = \frac{\alpha \operatorname{sgn}(\epsilon_s)}{\tilde{t}} = \frac{I}{\tilde{t}} \tag{26}$$

The s-wave susceptibility is simply

$$\chi_s = \sum_I N(0) \int_{-\omega_{sf}}^{\omega_{sf}} d\epsilon_I \left(\frac{\tanh\left(\frac{\beta \epsilon_I}{2}\right)}{2\epsilon_I} \right) \approx \sum_I N(0) \ln \left(\frac{\omega_{sf}}{2\pi T_c} \right). \tag{27}$$

When the electron and hole bands are present, $\sum_I = 2$, but when we hole dope the system the $I = -1$ term can be dropped, and we write $\sum_I \rightarrow 1$. The Josephson coupling between the two d-wave condensates is

$$\begin{aligned}\chi_{12} &= \sum_{I=\pm 1} N(0) \int_{-\omega_{sf}}^{\omega_{sf}} d\epsilon_I \left(\frac{\tanh\left(\frac{\beta\epsilon_I}{2}\right)}{2\epsilon_I} \right) \frac{I\tilde{t}^2}{\tilde{t}(\epsilon_I + I\tilde{t})} \int_0^{2\pi} \frac{d\theta}{2\pi} (\sin^2(2\theta) \cos^2(2\theta)) \\ &= \sum_I \frac{N(0)}{8} \int_{-\omega_{sf}}^{\omega_{sf}} d\epsilon_I \left(\frac{\tanh\left(\frac{\beta\epsilon_I}{2}\right)}{2\epsilon_I} \right) \frac{\tilde{t}^2}{\tilde{t}(I\epsilon_I + \tilde{t})} \approx \sum_I \frac{N(0)}{8} \ln\left(\frac{\omega_{sf}}{2\pi T_c}\right)\end{aligned}\quad (28)$$

Note that the contributions from the electron and hole bands add together. Similarly, for the Josephson coupling between the s- and d-wave order parameters we obtain

$$\begin{aligned}\chi_{1s} &= - \sum_I \int_{\mathbf{k}} \left(\frac{\tanh\left(\frac{\beta\epsilon_I}{2}\right)}{2\epsilon_I} \right) \left(\frac{I}{\epsilon_s \tilde{t}} \right) \epsilon_{xy} \epsilon_s d_{xy} \\ &= - \sum_I I N(0) \int_{-\omega_{sf}}^{\omega_{sf}} d\epsilon_I \left(\frac{\tanh\left(\frac{\beta\epsilon_I}{2}\right)}{2\epsilon_I} \right) \int \frac{d\theta}{2\pi} \sin^2(2\theta) \\ &= - \sum_I \frac{N(0)}{2} I \int_{-\omega_{sf}}^{\omega_{sf}} d\epsilon_I \left(\frac{\tanh\left(\frac{\beta\epsilon_I}{2}\right)}{2\epsilon_I} \right) \approx - \sum_I I \left[\frac{N(0)}{2} \ln\left(\frac{\omega_{sf}}{2\pi T_c}\right) \right]\end{aligned}\quad (29)$$

and similarly, omitting the intermediate steps,

$$\chi_{2s} = - \sum_I I \left[\frac{N(0)}{2} \ln\left(\frac{\omega_{sf}}{2\pi T_c}\right) \right]. \quad (30)$$

so the d-s couplings have *equal and opposite* contributions from the two helical bands. When both bands cross E_F , $\chi_{1s} = \chi_{2s} = 0$ and thus $\chi_{12}^{eff} = \chi_{12} > 0$, driving the system into the energetically favored s^\pm state. However, this compensation fails when the electron band is doped away from E_F , leaving behind the sole contribution from $I = +1$, so that $\chi_{1s} = \chi_{2s} = -(N(0)/2) \ln\left(\frac{\omega_{sf}}{2\pi T}\right)$. Substituting (27), (28), (29) and (30) into (19), we then obtain

$$\chi_{12}^{eff} = N(0) \ln\left(\frac{\omega_{sf}}{2\pi T_c}\right) \times \begin{cases} \frac{1}{4} & \text{(electron and hole pockets),} \\ -\frac{1}{8} & \text{(hole pockets only).} \end{cases} \quad (31)$$

Thus, at the Lifshitz point where the electron pockets disappear, the Coulomb repulsion causes a sign change in χ_{12}^{eff} and a first-order phase transition from the s^\pm to the octet state will then occur.

II. ORBITAL ANISOTROPY IN SUPERCONDUCTING PHASE

The orbital Rashba field mixes the orbital quantum numbers of the quasi-particles in the normal state, and the \vec{k} -space dependence of the rotating $\vec{B}_{\mathbf{k}}$ vector drives a modulation in

the orbital character of the normal state quasi-particles. This shows up as a d_{xy} -dependence of the orbital anisotropy $I_3(\mathbf{k}) = n_{xz}(\mathbf{k}) - n_{yz}(\mathbf{k})$, which has been measured experimentally in polarization-dependent ARPES[1].

However, the orbital Rashba field is modified by Andreev scattering upon condensation into the superconducting phase as the underlying d -wave orbital triplets will have a different orbital entanglement from the normal-state quasi-particles, i.e. $\vec{d}_{\mathbf{k}} \neq \vec{B}_{\mathbf{k}}$. Hence, the effective Rashba field in the superconducting phase picks up an additional $\vec{d}_{\mathbf{k}} \times (\vec{B}_{\mathbf{k}} \times \vec{d}_{\mathbf{k}}) \cdot \vec{\alpha}$ component, giving rise to a $\sin(2\theta) \sin(4\theta) \sim \cos(6\theta)$ component in the orbital anisotropy $I_3(\mathbf{k})$ that can also be measured in polarization-dependent ARPES.

The Hamiltonian of the system is given by,

$$\begin{aligned} H &= \sum_{\mathbf{k}} \psi_{\mathbf{k}\alpha\sigma}^\dagger (\mathcal{H}_{\mathbf{k}}^0 + \mathcal{H}_{\mathbf{k}}^{sc}) (i\sigma^2 \psi_{\mathbf{k}\alpha\sigma}) \\ \mathcal{H}_{\mathbf{k}}^0 &= (\epsilon_{\mathbf{k}} \mathbf{1} - \vec{B}_{\mathbf{k}} \cdot \vec{I}) \gamma^3 \\ \mathcal{H}_{\mathbf{k}}^{sc} &= \vec{d}_{\mathbf{k}} \cdot \vec{I} \gamma^1 \end{aligned} \quad (32)$$

and the orbital anisotropy can be calculated from the full Green's function of the system,

$$\begin{aligned} \mathcal{G}(\mathbf{k}, \omega) &= \frac{1}{\omega - H_{\mathbf{k}}^0 + H_{\mathbf{k}}^{sc}} \\ &= \frac{1}{\omega - (\epsilon_{\mathbf{k}} \gamma_3 - \vec{B}_{\mathbf{k}} \cdot \vec{I} \gamma_3 + \vec{d}_{\mathbf{k}} \cdot \vec{I} \gamma_1)} \\ &= \left(\omega + (\epsilon_{\mathbf{k}} - \vec{B}_{\mathbf{k}} \cdot \vec{I}) \gamma_3 + \vec{d}_{\mathbf{k}} \cdot \vec{I} \gamma_1 \right) \\ &\quad \times \frac{(\omega^2 - (\epsilon_{\mathbf{k}}^2 + |\vec{B}_{\mathbf{k}}|^2 + |\vec{d}_{\mathbf{k}}|^2) - 2\epsilon_{\mathbf{k}} \vec{B}_{\mathbf{k}} \cdot \vec{I} + 2\vec{B}_{\mathbf{k}} \times \vec{d}_{\mathbf{k}} \cdot \vec{I} \gamma_2)}{\left[\omega^2 - (\epsilon_{\mathbf{k}}^2 + |\vec{B}_{\mathbf{k}}|^2 + |\vec{d}_{\mathbf{k}}|^2) \right]^2 - 4\epsilon_{\mathbf{k}}^2 |\vec{B}_{\mathbf{k}}|^2 - 4|\vec{B}_{\mathbf{k}} \times \vec{d}_{\mathbf{k}}|^2} \end{aligned} \quad (33)$$

where we first multiply both numerator and denominator by the factor $(\omega + (\epsilon_{\mathbf{k}} + \vec{B}_{\mathbf{k}} \cdot \vec{I}) \gamma_3 + \vec{d}_{\mathbf{k}} \cdot \vec{I} \gamma_1)$ to trace out the γ_3 component. To trace out the orbital matrix \vec{I} components, we next multiply by $(\omega^2 - (\epsilon_{\mathbf{k}}^2 + |\vec{B}_{\mathbf{k}}|^2 + |\vec{d}_{\mathbf{k}}|^2) - 2\epsilon_{\mathbf{k}} \vec{B}_{\mathbf{k}} \cdot \vec{I} + 2\vec{B}_{\mathbf{k}} \times \vec{d}_{\mathbf{k}} \cdot \vec{I} \gamma_2)$. We finally obtain the expression for $\mathcal{G}(\mathbf{k}, \omega)$, with a denominator that is proportional to identity $\mathbf{1}$,

$$\begin{aligned} \mathcal{G}(\mathbf{k}, \omega) &= \left(\omega + (\epsilon_{\mathbf{k}} - \vec{B}_{\mathbf{k}} \cdot \vec{I}) \gamma_3 + \vec{d}_{\mathbf{k}} \cdot \vec{I} \gamma_1 \right) \\ &\quad \times \frac{(\omega^2 - (\epsilon_{\mathbf{k}}^2 + |\vec{B}_{\mathbf{k}}|^2 + |\vec{d}_{\mathbf{k}}|^2) - 2\epsilon_{\mathbf{k}} \vec{B}_{\mathbf{k}} \cdot \vec{I} + 2\vec{B}_{\mathbf{k}} \times \vec{d}_{\mathbf{k}} \cdot \vec{I} \gamma_2)}{(\omega^2 - (E_{\mathbf{k}}^-)^2) (\omega^2 - (E_{\mathbf{k}}^+)^2)} \end{aligned} \quad (34)$$

where,

$$E^\alpha(\mathbf{k}) = \left[(\epsilon_{\mathbf{k}}^2 + |\vec{B}_{\mathbf{k}}|^2 + |\vec{d}_{\mathbf{k}}|^2) - \alpha \sqrt{4\epsilon_{\mathbf{k}}^2 |\vec{B}_{\mathbf{k}}|^2 + 4|\vec{B}_{\mathbf{k}} \times \vec{d}_{\mathbf{k}}|^2} \right]^{1/2} \quad (35)$$

Multiplying out the terms in the numerator of $\mathcal{G}(\mathbf{k}, \omega)$, we see that there is an additional contribution to the orbital Rashba field in the superconducting state, $\delta \vec{B}_{\mathbf{k}} \propto (\vec{d}_{\mathbf{k}} \cdot \vec{I}_{\gamma_1})(\vec{B}_{\mathbf{k}} \times \vec{d}_{\mathbf{k}} \cdot \vec{I}_{\gamma_2})$ and using the Fierz identity $\sigma^a \sigma^b = i\epsilon^{abc} \sigma^c$, we obtain $\delta \vec{B}_{\mathbf{k}} = \vec{d}_{\mathbf{k}} \times (\vec{B}_{\mathbf{k}} \times \vec{d}_{\mathbf{k}}) \cdot \vec{I}_{\gamma_3}$. The effective orbital Rashba field component in $\mathcal{G}(\mathbf{k}, \omega)$ is then given by,

$$\mathcal{G}(\mathbf{k}, \omega) = \dots + \frac{-\vec{B}_{\mathbf{k}} \cdot \vec{I}_{\gamma_3} + \vec{d}_{\mathbf{k}} \times (\vec{B}_{\mathbf{k}} \times \vec{d}_{\mathbf{k}}) \cdot \vec{I}_{\gamma_3}}{(\omega^2 - (E_{\mathbf{k}}^-)^2)(\omega^2 - (E_{\mathbf{k}}^+)^2)} \quad (36)$$

We project into the particle (hole) basis by $P_{p(h)} = \frac{1}{2}(1 \pm \gamma_3)$, and the difference in the orbital occupancy between the xz and yz orbitals is given by I_3 . Hence, the orbital anisotropy is given by,

$$I_3(\mathbf{k}) = \frac{1}{\pi} \int_{-D}^0 \text{Im} \left[\text{Tr} \left(\mathcal{G}(\mathbf{k}, \omega - i\delta) \frac{(1 + \gamma_3)}{2} I_3 \right) \right] \quad (37)$$

where the integral is done only over the hole pocket around Γ , hence we choose a lower cut-off of $D = \frac{E^+(\mathbf{k}) + E^-(\mathbf{k})}{2}$. Note that the electron and hole pockets have opposite helicities, and integrating over both pockets will have canceling contributions.

Substituting Eq. 34 into Eq. 37, the shift in orbital anisotropy due to Andreev scattering is given by,

$$\begin{aligned} \delta I_3(\mathbf{k}) &= \int_{-D}^0 \frac{d\omega}{\pi} \text{Im} \left[\frac{\vec{d}_{\mathbf{k}} \times (\vec{B}_{\mathbf{k}} \times \vec{d}_{\mathbf{k}}) \cdot I_3}{(\omega^2 - (E_{\mathbf{k}}^-)^2)(\omega^2 - (E_{\mathbf{k}}^+)^2)} \right] \\ &= \int_{-D}^0 \frac{d\omega}{\pi} \frac{\vec{d}_{\mathbf{k}} \times (\vec{B}_{\mathbf{k}} \times \vec{d}_{\mathbf{k}}) \cdot I_3}{((E_{\mathbf{k}}^+)^2 - (E_{\mathbf{k}}^-)^2)} \text{Im} \left[\frac{1}{(\omega^2 - (E_{\mathbf{k}}^-)^2)} - \frac{1}{(\omega^2 - (E_{\mathbf{k}}^+)^2)} \right] \end{aligned} \quad (38)$$

Since we pick up only the poles in the lower helical band $E_{\mathbf{k}}^-$ due to a lower cut-off of D , this gives,

$$\begin{aligned} \delta I_3(\mathbf{k}) &= \int_{-D}^0 \frac{d\omega}{\pi} \frac{\vec{d}_{\mathbf{k}} \times (\vec{B}_{\mathbf{k}} \times \vec{d}_{\mathbf{k}}) \cdot I_3}{((E_{\mathbf{k}}^+)^2 - (E_{\mathbf{k}}^-)^2)} \text{Im} \left[\frac{1}{2E_{\mathbf{k}}^-} \left(\frac{1}{\omega - i\delta - E_{\mathbf{k}}^-} - \frac{1}{\omega - i\delta + E_{\mathbf{k}}^-} \right) \right] \\ &\approx \frac{1}{4|\epsilon_{\mathbf{k}}||\vec{B}_{\mathbf{k}}|} \frac{\vec{d}_{\mathbf{k}} \times (\vec{B}_{\mathbf{k}} \times \vec{d}_{\mathbf{k}}) \cdot I_3}{2\Delta_{sc}(\mathbf{k})} \end{aligned} \quad (39)$$

Thus, the Andreev shift of the Rashba field gives a signal $\delta I_3(\mathbf{k})$ of $O(\frac{\Delta}{|\epsilon_{\mathbf{k}}|})$, and we have approximated the superconducting gap in the quasi-particle basis by,

$$\Delta_{sc}^2(\mathbf{k}) \approx |\vec{d}_{\mathbf{k}}|^2 - \frac{|\vec{B}_{\mathbf{k}} \times \vec{d}_{\mathbf{k}}|^2}{|\epsilon_{\mathbf{k}}||\vec{B}_{\mathbf{k}}|} \quad (40)$$

and, we have approximated $E^\pm(\mathbf{k}) \approx \left[\left(\epsilon_{\mathbf{k}} \pm |\vec{B}_{\mathbf{k}}| \right)^2 + \Delta_{sc}^2(\mathbf{k}) \right]^{1/2} \approx \Delta_{sc}(\mathbf{k})$, and $(E_{\mathbf{k}}^+)^2 - (E_{\mathbf{k}}^-)^2 = 2\sqrt{4\epsilon_{\mathbf{k}}^2|\vec{B}_{\mathbf{k}}|^2 + 4|\vec{B}_{\mathbf{k}} \times \vec{d}_{\mathbf{k}}|^2} \approx 4|\epsilon_{\mathbf{k}}||\vec{B}_{\mathbf{k}}|$ near the hole and electron pocket Fermi surfaces.

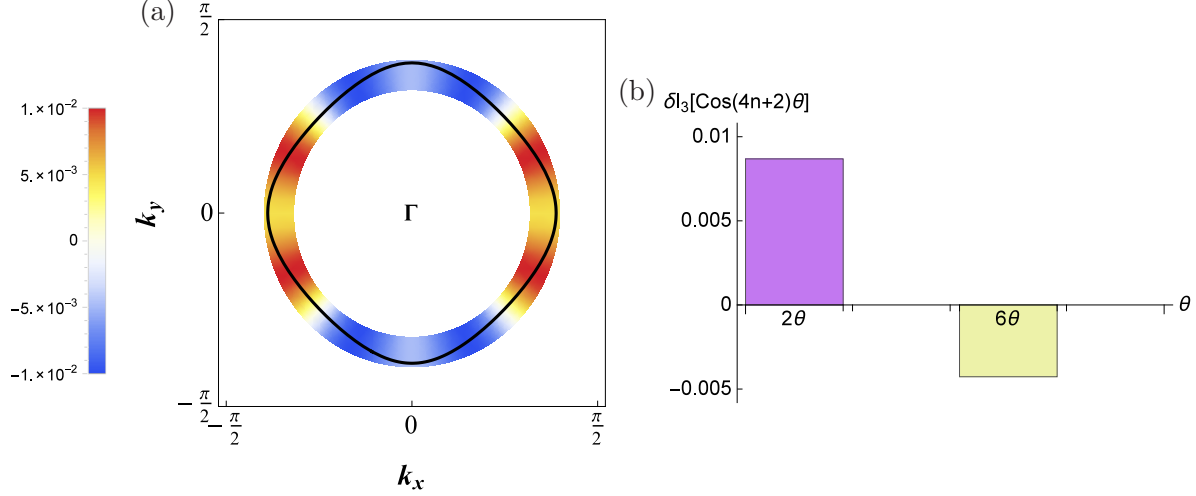


FIG. 1: Density plot of shift in orbital anisotropy $\delta I_3(\mathbf{k}) = I_3^{sc}(\mathbf{k}) - I_3^n(\mathbf{k})$. This is the case when $|\Delta_{xy}| > |\Delta_{x^2-y^2}|$, and the s^\pm state shows a negative shift in $I_3(\mathbf{k})$, with a negative $\cos(6\theta)$ component and a positive $\cos(2\theta)$ Fourier component, as shown in Fig. (b).

We numerically evaluate Eq. 37, on a 200×200 grid in the upper right BZ quadrant $k_x, k_y \in [0, \pi/2, 0, \pi/2]$, and the energy integral over ω is carried out in Mathematica using an adaptive algorithm. The orbital anisotropies in the normal and s^\pm superconducting phase are plotted in Figs. 1 & 2, for the two cases of $|\Delta_{xy}| > |\Delta_{x^2-y^2}|$ and $|\Delta_{xy}| < |\Delta_{x^2-y^2}|$ respectively.

We also carry out a Fourier Transform of the orbital anisotropy signal $\delta I_3(\mathbf{k})$, and since $I_3 = \langle xz \rangle - \langle yz \rangle$, this means that $I_3 \in B_{1g}$ and it will have nodes along the diagonals, and also has to change sign upon R^{90° . Thus, the only Fourier components it will have are $\cos 2(2n+1)\theta$ components, and we show the first two components $\cos(2\theta)$ and $\cos(6\theta)$ which have the largest signals. The $\cos(2\theta)$ component will have the largest contribution from the Rashba field \vec{B}_{bk} , and the most interesting signal comes from the $\cos(6\theta)$ component that depends on the shift due to the double Andreev scattering process.

III. GAPLESS ANDREEV EDGE STATES

C_{4v} symmetry guarantees the degeneracy of the xz and yz orbitals, which allows the system to condense into an orbitally-entangled triplet state. This non-trivial entanglement

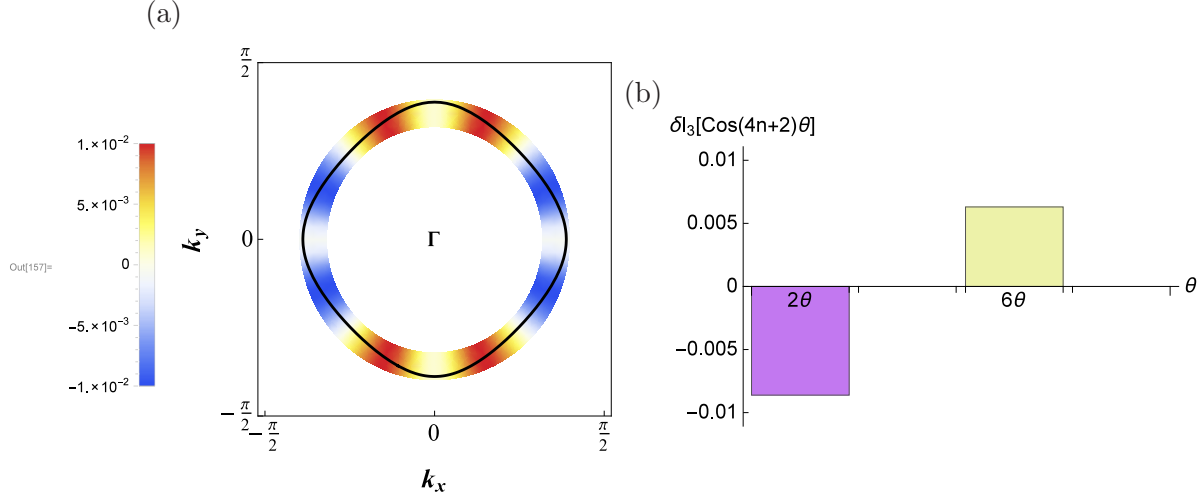


FIG. 2: Density plot of shift in orbital anisotropy $\delta I_3(\mathbf{k}) = I_3^{sc}(\mathbf{k}) - I_3^n(\mathbf{k})$. This is the case when $|\Delta_{xy}| < |\Delta_{x^2-y^2}|$, and the s^\pm state shows a positive shift in $I_3(\mathbf{k})$, with a positive $\cos(6\theta)$ component and a positive $\cos(2\theta)$ Fourier component, as shown in Fig. (b).

is reflected by the winding number of the $\vec{d}_{\mathbf{k}}$ vector, which we re-state here for convenience.

$$\oint_{\Gamma} \hat{z} \cdot (\vec{d}^\dagger(\mathbf{k}) \times \partial_a \vec{d}(\mathbf{k})) dk_a = 2\pi\nu \quad (41)$$

This orbitally entangled nature is reflected in the existence of gapless Andreev edge states at domain walls between two regions with different topological numbers ν . Here, we calculate the edge states at the domain wall between two bulk orbital triplet states of opposite chirality, with a boundary at $x = 0$ and satisfying the boundary conditions $\Delta_2(x = -\infty) = -\Delta_2$ and $\Delta_2(x = \infty) = +\Delta_2$, using the method described by Volovik [2]. The winding number ν (Eq. 41) changes sign from $+2$ to -2 across the domain, when $\Delta_2(x)$ changes sign. However, the orbital Rashba vector $\vec{n}_{\mathbf{k}}$ remains unchanged across the domain wall, hence the system is in the “low”-spin s^\pm state on the left, and in the “high”-spin octet state on the right of the domain wall.

For small $k_x^2 \ll k_F^2$, we can calculate the edge states perturbatively. Letting $k_x = k_F + i\partial_x$, $\epsilon_{xy} = \frac{t_1}{k_F^2} k_x k_y$ and $\epsilon_{x^2-y^2} = \frac{t_3}{k_F^2} (k_x^2 - k_y^2)$, we obtain the Hamiltonian,

$$H = H^{(0)} + H' \quad (42)$$

$$H^{(0)} = iv_F \partial_x \gamma_3 + t_3 I_3 \gamma_3 + \Delta_2(x) I_3 \gamma_1 \quad (43)$$

$$H' = \frac{\Delta_1}{k_F} k_y I_1 \gamma_1 + \frac{t_1}{k_F} k_y I_1 \gamma_3 \quad (44)$$

where $v_F = \frac{k_F}{m}$. H acts on Nambu spinor,

$$\psi_{\mathbf{k}I\sigma} = \begin{pmatrix} c_{\mathbf{k}xz,\uparrow} \\ c_{\mathbf{k}yz,\uparrow} \\ c_{-\mathbf{k}yz,\downarrow}^\dagger \\ -c_{-\mathbf{k}xz,\uparrow}^\dagger \end{pmatrix} \quad (45)$$

over half the $BZ \in \vec{k} > 0$. Since the Cooper pairs are also spin singlets, there is an additional spin degree of freedom that gives rise to a degenerate Nambu spinor,

$$\psi'_{\mathbf{k}I\sigma} = \begin{pmatrix} c_{\mathbf{k}xz,\downarrow} \\ c_{\mathbf{k}yz,\downarrow} \\ -c_{-\mathbf{k}yz,\uparrow}^\dagger \\ c_{-\mathbf{k}xz,\downarrow}^\dagger \end{pmatrix} \quad (46)$$

Thus, we can choose to carry out our calculations using only $\psi_{\mathbf{k}I\sigma}$ over the full BZ , which is equivalent to calculations using both $\psi_{\mathbf{k}I\sigma}$ and $\psi'_{\mathbf{k}I\sigma}$ over half the BZ .

Since $[I_3 \mathbf{1}, I_3 \gamma_2] = 0$, we can find two zero-energy solutions $H |\psi\rangle = 0$,

$$\begin{aligned} \psi_\pm(x) &= \exp \left[-\frac{1}{v_F} \int_0^x dx' (\Delta_2(x') I_1 \gamma_1 - i t_3 \alpha_3 \gamma_3) \right] \xi_\pm, \\ \xi_+ &= \begin{pmatrix} 1 \\ 0 \\ i \\ 0 \end{pmatrix}, \quad \xi_- = \begin{pmatrix} 0 \\ 1 \\ 0 \\ -i \end{pmatrix} \end{aligned} \quad (47)$$

Hence, we see that the edge states have a decay length given by $\frac{1}{l} = \frac{\Delta_2}{v_F}$, and the Fermi momentum along k_x is shifted by $\pm \frac{t_3}{v_F}$ for ξ_\pm respectively due to the Rashba coupling. We now treat the edge Hamiltonian H' as a perturbation, and acting in the subspace of ξ_\pm , this gives

It is straightforward to show that the zero-energy modes satisfy the following Hamiltonian along the edge, and disperse linearly.

$$\begin{bmatrix} H'_{++} & H'_{+-} \\ H'_{-+} & H'_{--} \end{bmatrix} = \begin{bmatrix} 0 & vk_y + i\delta k_y \\ vk_y - i\delta k_y & 0 \end{bmatrix} \quad (48)$$

where,

$$v = \frac{t_1}{k_F}, \quad \delta = \frac{\Delta_1}{k_F} \quad (49)$$

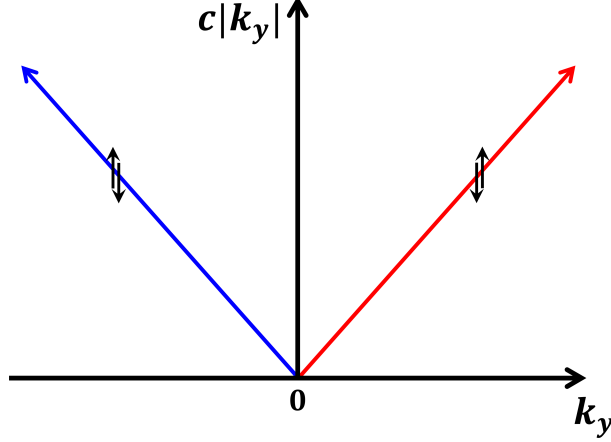


FIG. 3: Gapless Andreev Edge States. Linearly dispersing gapless Andreev edge states occur at the domain wall between a “low”-spin s^\pm state and a “high”-spin octet state. These edge states carry a definite angular momentum of $\langle L_z \rangle = \pm 1$ for the left and right movers. Due to the spin singlet nature of the Cooper pairs, these edge states are also doubly degenerate in spin-space, with a pair of spin-polarized left movers, and another pair of spin-polarized right-movers.

Solving the edge Hamiltonian, Eq. 42, gives the following two fermionic zero modes,

$$\begin{aligned} H' \psi_{L,R} &= \pm c k_y \psi_{L,R} \\ c &= \sqrt{v^2 + \delta^2} \end{aligned} \quad (50)$$

where $\psi_{1,2}$ are two linearly dispersing gapless Andreev bound states. As $\psi_{\mathbf{k}I\sigma}$ and $\psi'_{\mathbf{k}I\sigma}$ are spin-polarized states with spin up and down respectively, we get two sets of gapless Andreev bound states with definite spin and orbital iso-spin, but these Andreev edge states are not Majorana fermions as they are spin-polarized.

-
- [1] Y. Zhang, F. Chen, C. He, B. Zhou, B. P. Xie, C. Fang, W. F. Tsai, X. H. Chen, H. Hayashi, J. Jiang, H. Iwasawa, K. Shimada, H. Namatame, M. Taniguchi, J. P. Hu, and D. L. Feng, Phys. Rev. B **83**, 054510 (2011).
[2] G. Volovik, JETP Letters **90**, 398 (2009).